Journal of Crystal Growth 653 (2025) 128067

Contents lists available at ScienceDirect

Journal of Crystal Growth

journal homepage: www.elsevier.com/locate/jcrysgro

About crystal growth of hybrid bromide perovskite single crystals

Silvia Rizzato [a,b,*], Marianna Testa [b], Massimo Moret [c]

[a] Dipartimento di Chimica, Università degli Studi di Milano, Milano, Italy
[b] Istituto Nazionale di Fisica Nucleare (INFN), Laboratori Nazionali di Frascati, Frascati, Italy
[c] Dipartimento di Scienza dei Materiali, Università degli Studi di Milano-Bicocca, Milano, Italy

ARTICLE INFO

Communicated by Keshra Sangwal

Keywords:
Hybrid lead halide perovskite
Crystallization
Single crystals
Inverse−temperature crystallization (ITC) method
Self-healing capability
Halide ion exchange

ABSTRACT

The most conventional way to grow centimetres sized $MAPbBr_3$ (MA = methyl ammonium) perovskite single crystals is the temperature rising method from dimethylformamide solution in which $MAPbBr_3$ shows an inverse solubility/T dependence. In the present study a well-defined crystallization procedure was provided. The collective and individual effect of the many experimental variables involved were highlighted and a set of guidelines were produced to control nucleation, crystal size and the macro/micro-morphology of the crystals. Several critical aspects connected to the process or environmental conditions, such as moisture level or total reaction time, have been revealed and investigated to ensure high products reproducibility between batches and over time. The efficient self-healing capability of $MAPbBr_3$ single crystals has been confirmed and exploited to induce a regeneration process.

1. Introduction

Organometal halide perovskites (OMHP) have emerged as a promising class of semiconductors for application in photovoltaic and optoelectronic devices due to their considerable and tunable optical and electronic properties [1]. Several synthesis procedures have been developed to easily prepare perovskite systems in different structural shape and geometries, such as single crystals [2,3], thin films [4,5] and nanostructured products like nanowires, quantum dots [6] or nanocrystals [7,8]. Each of these forms exhibits unique properties that make them suitable for specific application or specific device configurations.

Despite their impressive features, including chemical flexibility, synthetic versatility and defect tolerance [9], there are several challenges that need to be addressed for a successful practical application of hybrid perovskites and their widespread adoption. The main concerns are the poor long-term stability and durability of these materials that can degrade in the presence of moisture and heat, their energy-storage efficiency and environmental toxicity but also a lack of standardized procedures for preparing samples, evaluating degradation factors and performing reliable efficiency measurements [10,11].

As a rule, perovskite single crystals are known to exhibit higher electronic performance than their polycrystalline counterparts resulting from unique long carrier dynamics due to a lower concentration of defects and the absence of grain boundaries [12]. The same behaviour has been observed for silicon devices although it remains unclear how the interplay between macro and micro-structure can affect the performance and stability of the OMHP devices [13]. Further advantages of single crystals are their anisotropy, that enables measurement and use of crystal-direction dependent properties, and their high level of optical homogeneity. In addition, some large-size hybrid perovskites crystals have shown a remarkable self-healing capability with the recovery of damaged areas and/or the electronic and optical properties that provide a way to extend lifetime and regenerate these materials. The most conventional way to obtain large-size OMHP single crystals with a fast-growing rate and low cost is the temperature rising method [14,15], that for $MAPbBr_3$ (methyl ammonium lead bromide) perovskite relies on the inverse solubility behaviour of this specie in DMF (N,N-dimethylformamide). However, despite the numerous experimental data available in the literature, no well-defined, highly reproducible, and easily adjustable procedures have been outlined.

To optimize the cost of the process and improve the control on the size, morphology and the macroscopic defectiveness of the crystals, a thorough investigation has been performed considering all the possible variables involved. Several critical aspects have been revealed and evaluated such as the starting material, the type of vessel and the process lead time. A simple but accurate crystal growth procedure has been developed to control nucleation, crystal size and morphology of the crystals optimizing time and yield. The procedure has also proved to be

* Corresponding author.
E-mail address: silvia.rizzato@unimi.it (S. Rizzato).

https://doi.org/10.1016/j.jcrysgro.2025.128067
Received 22 October 2024; Received in revised form 9 January 2025; Accepted 11 January 2025
Available online 13 January 2025

an efficient and effective strategy for achieving a successful reconstitution of broken or damaged single crystals.

Some phenomena related to environmental and process conditions such as air-moisture and solvent hydration that can have detrimental effects on the material properties and, consequently, on material performance, were also highlighted and discussed. Due to its effectiveness the growth procedure has been used to produce the crystal used in the first perovskite-based device for the detection of high energy electron with a sensitivity down to a single particle [16].

2. Experimental section

2.1. Chemicals

Lead (II) bromide ($PbBr_2$, ≥ 99.99 %) and methylammonium bromide (MABr, ≥ 99.99 %) were purchased respectively from Aldrich and Greatcell Solar Materials. All the solvents (dichloromethane, chloroform, 1,2-dichloroethane, ether, ethyl acetate, tetrahydrofuran, methanol, ethanol, isopropanol, acetone, N,N-dimethylformamide, toluene) were purchased from commercial suppliers (Merck, Carlo Erba Reagents and VWR International) and were ACS, AR or HPLC grade with mass purities higher than 99.5 %. In particular, dichloromethane (DCM) was ACS reagent grade (Sigma-Aldrich), ≥ 99.9 %, whereas N,N-dimethylformamide (DMF) was RPE-ACS analytical grade reagent (Carlo Erba Reagents), ≥ 99.9 %. Epoxy resin and curing agent were purchased from Resin-Pro under the trade name One-to-One Flex (1:1).

2.2. Crystal growth

2.2.1. Crystal growth procedure

First step (preparation of seed crystals)**:** a solution of $MAPbBr_3$ in DMF at a concentration of about 1.2 M was prepared by dissolving 11.50 g of pure perovskite powder (see section 2.2.2 for preparation) in 20 mL of solvent transferred with a graduated pipette. The solution was kept under magnetic stirring at room temperature for about two hours after the complete dissolution of the reactant. The solution was filtered using a PTFE filter with 0.45 mm pore size and then poured into a 100 mL beaker (or a 150 mL Erlenmeyer flask). The flask was placed in a jacketed crystallizer (inner diameter 85 mm, inner length 140 or 100 mm) connected to a heating/cooling thermostat and covered with a glass watch to minimize solvent loss by evaporation and prevent contamination. The crystals were grown by temperature rising in the range of 50–88 °C according to a defined growth temperature program (see step 1 in Table 1). The resulting crystals were quickly recovered from the hot solution and dried in an oven at 45 °C for one day. Smaller vessel and upper or lower fill levels (10 mL, 30 mL) were tested. This step represents a convenient strategy to obtain medium-sized crystals (up to 4–6 mm) of good quality.

Second step (single crystal growth – seeding 1)**:** a solution of $MAPbBr_3$ in DMF at a concentration of about 1.0 M was prepared by dissolving 4.80 g of pure perovskite powder in 10 mL of solvent transferred with a graduated pipette. The solution was kept under magnetic stirring at room temperature for about two hours after complete dissolution of the compound was observed. The solution was filtered using a PTFE filter with 0.45 mm pore size and then poured into a 25 mL beaker (or a 25 mL Erlenmeyer flask). The vessel was placed in a jacketed crystallizer (inner diameter 55 or 60 mm, inner length 70 mm) connected to a heating/cooling thermostat set at 60 °C. The seeding was performed by placing a seed crystal at the bottom of the growing container using tweezers. The seed crystals used in the experiment (grown as described in step 1) have a plate-like shape and more than five millimetres in size (5 mm on a side and 1 mm thick) and are selected by observation under a polarized microscope. The process can be performed in two different configurations, one in which the crystal was oriented vertically and one in which the crystal is oriented horizontally (Fig. 1). The crystals were grown by temperature rising in the range of 60–80 °C according to a defined growth temperature program (see step 2 in Table 1). Secondary nucleation was sometimes observed but in limited extent and as expected at a lower saturation level than primary nucleation. At the end of the process the crystals were quickly recovered from the hot solution and dried in an oven at 45 °C for one day.

The first seeding (step 2) can be repeated successively on the same

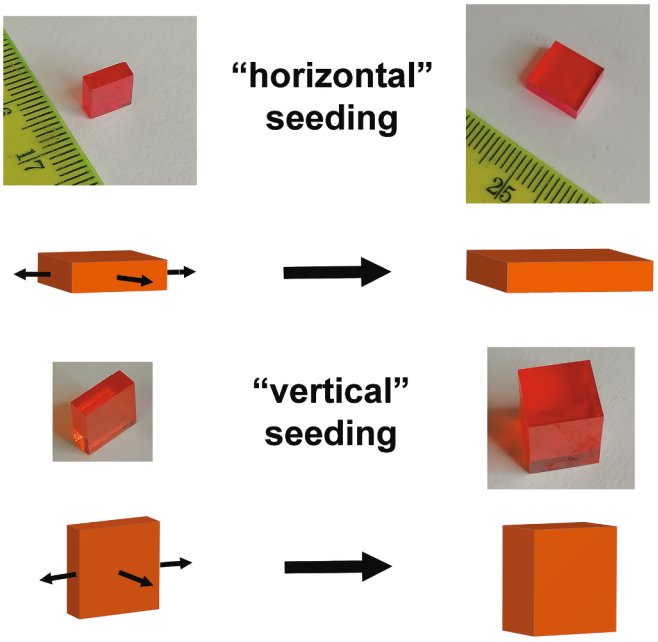

Fig. 1. Two different configurations for the seeding steps: one in which the crystal is oriented vertically (size in cm: 0.10 × 0.95 × 0.5) and one in which the crystal is oriented horizontally (size in cm: 0.90 × 0.85 × 0.35). The final shape of the crystals results strongly influenced by the orientation of the seed crystals.

Table 1
Growth temperature program for the three steps of the crystal growth procedure.

STEP 1				STEP 2				STEP 3			
	T (°C)	Time (minutes)	Heating rate (°C/h)		T (°C)	Time (minutes)	Heating rate (°C/h)		T (°C)	Time (minutes)	Heating rate (°C/h)
1	50	10	0.00	**1**	60	10	0.00	**1**	35	10	0.00
2	55	30	10.00	**2**	62.5	20	7.50	**2**	40	200	1.50
3	57	400	0.30	**3**	65	400	0.38	**3**	45	1000	0.30
4	60	900	0.20	**4**	70	450	0.67	**4**	50	1500	0.20
5	65	400	0.75	**5**	75	250	1.20	**5**	60	800	0.75
6	70	200	1.50	**6**	80	80	3.75				
7	80	120	2.50								
8	85	40	7.50								
9	88	20	9.00								
		Tot. 2120				Tot. 1210				Tot. 3510	

crystal even if the starting size of the crystal is clearly larger. The result will be different from that obtained applying the full growth procedure (lower crystal quality and lower crystal yield), i.e. including the third step.

Third step (single crystal growth – seeding 2)**:** a solution of $MAPbBr_3$ in DMF at a concentration of about 1.5 M was prepared by dissolving 7.18 g of pure perovskite powder in 10 mL of solvent transferred with a graduated pipette. The solution was kept under magnetic stirring at room temperature for about two hours after complete dissolution of the compound was observed. The solution was filtered using a PTFE filter with 0.45 mm pore size and then poured into a 25 mL beaker (or a 25 mL Erlenmeyer flask). The vessel was placed in a jacketed crystallizer (inner diameter 55 or 60 mm, inner length 70 mm) connected to a heating/cooling thermostat set at 35 °C. The seeding was performed by placing a seed crystal at the bottom of the growing container using tweezers. The seed crystals used in the experiment (grown as described in the step 2) have a flattened prismatic shape and more than eight millimetres in size (8 mm on a side and 3 mm thick). As in the first seeding, the process can be performed with the prismatic crystal vertically or horizontally oriented. The crystals were grown by temperature rising in the range of 35–60 °C according to a defined growth temperature program (see step 3 in Table 1). Secondary nucleation was sometimes observed in the temperature range 43–48 °C but in limited extent and far from the seed crystal. At the end of the process the crystals were quickly recovered from the hot solution and dried in an oven at 45 °C for one day.

2.2.2. Preparation of $MAPbBr_3$ precursor

Crystalline powders of perovskite were produced by antisolvent method starting from a stoichiometric solution of the precursors at a concentration of about 1.0 M. 4.50 g MABr were weighed in a beaker, mixed with 40.0 mL of DMF and magnetically stirred until completely dissolved. The appropriate amount of $PbBr_2$ (14.70 g) was weighed into another beaker and added in portions to the former solution under stirring. The solution was then poured into a 150 mL Erlenmeyer flask before the addition of 60 mL of pure antisolvent. The resulting mixture was kept under vigorous magnetic stirring for at least one hour. The precipitate (orange solid) was recovered by filtration under vacuum, washed twice by using the antisolvent and dried in an oven for 12–24 h at 45 °C. To confirm the purity and crystallinity nature of the material all the samples were ground and characterized by X-ray powder diffraction. A variety of solute concentrations, antisolvents and solvent/antisolvent ratios have been tested to optimize yield, purity, and crystallinity of the product but also to ensure an easier sample recovery and handling:

– Antisolvent: dichloromethane, chloroform, 1,2-dichloroethane, methanol, ethanol, isopropanol, diethyl ether, ethyl acetate, tetrahydrofuran, acetone, toluene.

– $CH_3NH_3PbBr_3$ ($MAPbBr_3$) molar concentration: 0.5 M, 1.0 M, 1.5 M.

– Antisolvent/solvent volume ratio: 2.5, 2.0, 1.5, 1.0.

The best results were obtained by using diethyl ether as antisolvent. The preparation of perovskite powder was repeated at least 30 times for each “good” cosolvent (dichloromethane, chloroform, diethyl ether) to obtain a reliable estimate of the yield (average yield for ether: 90 %).

2.2.3. Antisolvent effect

A short crystallization screening for the $MAPbBr_3$ system was accomplished using the liquid/liquid diffusion or layering technique. All the crystallization trials were performed in a glass tube of length 100 mm and inner diameter 10 mm, by layering a poor solvent (3.0 mL) and a perovskite solution in DMF (2.0 mL) on top of each other. The screening was performed by changing the solute concentration ($0.06 < [MAPbBr_3] < 0.12$ M) and the nature of antisolvent system (dichloromethane, chloroform, 1,2-dichloroethane, ether, ethyl acetate, tetrahydrofuran, methanol, toluene). All samples were left to stand at room temperature and constantly monitored, by using an optical microscope (Olympus SZX16). In the samples containing dichloromethane solvent a visible change in the colour of crystals was observed over a relatively long time. The colour gradually moves from dark orange to light orange ending with yellow-orange or bright yellow without any degradation or changes in the macroscopic morphology of the crystals or in the powder aspect. To better understand the phenomenon some experimental verifications were conducted by exposing the perovskite in form of powder or DMF solution to a chlorinated solvent: (a) about 200 mg of perovskite was transferred into a 25 mL round bottom flask and covered with 10 mL of pure dichloromethane or 10 mL of a DMF-CH_2Cl_2 mixture (40:60 ratio); (b) liquid/liquid diffusion trials were performed by layering in a test-tube 2 mL of a 0.1 M perovskite solution in DMF over 3 mL of pure dichloromethane. Three sets of a and b samples were prepared and kept under different conditions: in the dark, under light, at ambient or low (3–4 °C) temperatures.

2.3. Characterization of crystals

Powder diffraction experiments were carried out to confirm the halide exchange into the perovskite structure and determine the chlorine percentage in the samples (see supplementary material, section S2). All precipitates, in the form of powder or single crystals, were recovered from any screening test, air dried, finely ground, and loaded as such on the sample holder to ensure that all parts of the sample are evenly represented. All the samples were stored at ambient conditions for at least three months before being removed and analysed via XRD. Ambient X-ray powder diffraction measurements were performed using a Miniflex-600 diffractometer (Rigaku, Japan) with Cu K_α (λ = 1.540598 Å) radiation over the angular range of 5-60° (2θ), with an incremental step size of 0.02° (2θ) and a counting time of 1 or 2 s·step^{-1}. Analysis of XRD data was done by using *FullProf* suite software [17]. The simulated powder patterns were calculated using the crystallographic information files (CIFs) from single-crystal X-ray experiments. Phase identification was performed by comparing the experimental data with those stored in the reference database (CCDC). [18].

The growth process of perovskite monocrystals was recorded using a digital microscope with 200x total magnification (RS PRO USB Digital Microscope). Optical observations were made with a polarizing SZX16 Olympus stereomicroscope.

3. Results and discussion

3.1. Crystal growth procedure

The experimental procedure has been accurately designed to grow centimetre-sized organic–inorganic hybrid halide perovskite single crystals by the inverse temperature crystallization method (ITC) [14] from DMF and has been refined to eliminate unnecessary steps and reduce the procedure time while maximizing the process yield. Indeed, the outcome of a crystallization process can be greatly improved if the experimental settings are modified and fine-tuned throughout the process to reflect the different conditions required by the nucleation and the several stages of a growth process. To this purpose, the experimental procedure has been split into three distinct steps: a) the production of good quality seed crystals of a suitable size, b) the increase of crystals size by seeding method, c) the controlled change of the crystal shape by a second seeding stage.

The experiment setup and the procedure are described in detail in the experimental part. The crystal growth procedure is highly reproducible and can be easily modified. Only minor adjustments in the temperature program may be needed to account for slight differences in the operational setting (such as use of a jacketed crystallizer of different size). For each stage, several critical aspects have been highlighted and investigated including the size and shape of the crystallization vessel, the total volume of the crystallization solution and the vessel filling level.

In addition, numerous trials have been conducted to assess the effects of concentration, reaction time and reaction temperature on the

macroscopic imperfections and the growth morphology of the crystals. This systematic screening made it possible to identify the threshold parameters required to avoid unstable growth or high interfacial instability that are responsible for deformations of the crystals' surface with the appearance of characteristic hopper faces consisting of macro-steps [19]. It has been observed that too long reaction time and too high or too low reaction temperature favour the transition from cubic shape to hopper morphology [20], while an increase of $MAPbBr_3$ concentration results in a better morphological stability although this leads to a larger probability for new nucleation events to occur. On the other hand, the size of the crystals increases with the temperature and the source concentration. A similar behaviour has been observed for the analogous methylammonium lead iodide perovskite crystals grown by solvothermal methods [21].

Based on the experimental observations, which will be now discussed for each step, the growth procedure was amended several times to yield better results, and all the procedures were repeated number of times to ensure the reproducibility of the outcomes.

The first step of procedure has been devoted to preparing seed crystals of suitable size, but it also represents a convenient strategy to obtain medium-sized crystals (up to 4–6 mm) of good quality. The results are strongly affected by the vessel type and the solution volume. Large reaction vessels (100 and 150 mL) and a relatively small reaction volume (20 mL) work better than smaller vessels (50 mL) and lower or upper fill levels (10 to 30 mL). To limit the extent of nucleation density but also to induce a fast and extended growth of the crystallites, an increasing temperature rise rate needs to be employed (from 0.3 °C/h to 9.0 °C/h); furthermore, to ensure a good yield the final temperature of the process must be not too low (at least 85 °C). The crystal size distribution is quite uniform, and all the crystals show a cubic plate habit with a hopper face on the "bottom" side in contact with the crystallization vessel.

The next steps of procedure involve two sequential seeding processes that were designed to achieve a high mass ratio of final crystals to seeds (Fig. 1). In both steps the crystals magnify up to five times with a yield above 50 % and 55 % respectively, corresponding to a mass growth greater than 1 g (seeding 1) and 2 g (seeding 2).

The two seeding steps differ significantly in the starting concentration, temperature range and heating rate but can be interchanged by making appropriate changes to the ramp-up schemes. However, the different kinetics and mechanism of growth at work in the two stages (i.e. 2D nucleation and layer-by-layer growth), that are strictly connected to the supersaturation grade and the supersaturation change rate, can deeply affect the extent of the crystal growth but also the morphology and the surface features of the final crystals. Therefore, it must be pointed out that any changes in the procedure could have important effects on the final products.

All steps of the crystal growth procedure require the preparation of a $MAPbBr_3$ solution of appropriate concentration that can be obtained by dissolving the two precursors $PbBr_2$ and MABr in 1:1 M ratio in DMF. However, we observed that a better reproducibility and reliability of the results can be achieved only by using freshly prepared $MAPbBr_3$ salt. The pure perovskite powder to use as raw material has been easily and quickly produced by using the antisolvent precipitation method starting from a DMF solution of the precursors as described in the experimental part. A variety of antisolvents, solvent/antisolvent ratios and solute concentrations has been tested to optimize the yield, purity, and crystallinity of the product [22].

Beyond the development of the crystal growth procedure, several additional phenomena were observed that should be highlighted. First, in most cases, at the beginning of the seeding experiment a partial dissolution of the seed crystal occurs until the saturation point is reached. The dissolution takes place at very low-undersaturation starting from the exposed corners, edges and dislocation cores that represents the most favourable desorbing locations on the crystal surface [23]. The dissolution mechanism is responsible for the morphology deformation of the crystals that show a non-uniform surface retreat and a rounding of the edges (Movie S1 and S2) [24]. As a result, the top part of the crystal appears highly rough and dominated by macro-steps that nevertheless favour the easy and fast crystal reconstruction as soon as the solution becomes supersaturated.

The recovery process takes place by generation of growth steps and terraces on the deformed faces and continues until the faces and the edges are restored. The dominant mechanism at work in the restoration process is clearly the layer-by-layer growth that reveals a constant and helpful generation of a low supersaturation in solution with the increasing temperature provided by the procedure [25]. The same mechanism is responsible for the morphological reconstruction of the hopper and cracked seed crystals resulting in the restoration of their overall performance. In fact, in many cases the last step of the seeding process has allowed to recover partially or totally the spirally terraced pit of the hopper faces of the seed crystals leading to smoother surfaces. The restoration resulted so effective to produce gently sloped pyramidal faces or dislocation hillocks. Under the same conditions, broken or imperfect (damaged) crystals have shown a remarkable self-repairing capability resulting in a rapid filling of gaps and fast completion of the expected growth shape (Fig. 2, Fig. S1, Movie S3 and Movie S1). It is important to point out that no dependence of the extent and orientation of breakage on the crystal shape evolution was observed and reconstitution was successful on several samples with different mechanical damage.

This efficient capacity of halide perovskites for self-repair or self-heal photophysical or photochemical and mechanical damages has been demonstrated for both poly and single crystalline forms of methylammonium lead iodide ($MAPbI_3$) with the recovery of the photoluminescence properties of the material [26,27]. More recently, experimental evidence that corroborate the same damage-healing behaviour of perovskite materials also at nanoscale level have been presented [28]. Beyond the recovery process, the initial dissolution step is important because it could be useful to improve the quality of the crystalline phase, as observed for crystals of biological macromolecules grown by the solution-temperature method [29].

The reported findings are very interesting because they may have broad and important implications as the strategy could be generalized to extend the durability and sustainability of the functional devices based on hybrid perovskites.

3.2. Control of crystal morphology

Another important aspect concerns the effect of the initial seed crystal orientation on the final growth morphology [30]. Indeed, the seeding process can be performed by placing the cubic-plate seed crystal oriented either vertically or horizontally on the bottom of the

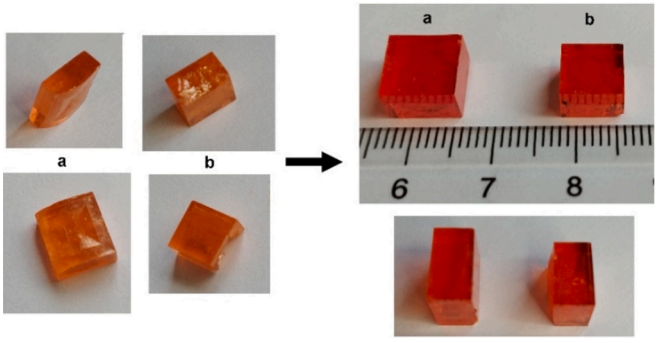

Fig. 2. A picture showing the recovery process and the crystal shape evolution involving broken or deformed crystal that takes place in the second seeding process. Reconstitution process is effective for both vertical and horizontal alignment of the seed crystal: a) crystal seeded horizontally, (b) crystal seeded vertically.

crystallizer. However, in the two cases, the effective seed surface area exposed to the solution, and thus accessible, is different, leading to different growth degree and morphological recovery of the crystals. Better results were obtained with the seed crystal vertically aligned (higher yield of about 10–15 %, more effective surface restoration). Moreover, since the growth can involve only the solution-facing sides of the crystals, by changing the orientation of the seeds is possible to shape the starting cubic plate into a few different configurations (thicker plate, perfect cube or rectangular prism; see Fig. 1). This is important because the external shape of the crystals can critically affect their functional properties but also their use in the processing of the devices.

3.3. Detrimental factors affecting crystal growth

The proposed growth procedure is very effective but requires paying attention to some detrimental factors affecting the quality, stability and efficiency of the products. These include ambient and operational parameters, such as humidity and chemical contaminations.

As described above, the precursor $MAPbBr_3$ material is prepared using an antisolvent-assisted strategy. A variety of antisolvents has been tested to optimize the process. The results show that most of the tested antisolvents work quite efficiently, but the best results were achieved with diethyl ether that ensures a high yield and an easily handled powder. Chlorinated solvents may represent a valuable alternative and are often used as precipitating agents to fabricate perovskite nanostructures or in perovskite deposition processes. However, we found that chlorinated systems provide samples difficult to dry and recover and, more importantly, can lead to phase impurities.

In fact, it has been shown that hybrid and inorganic halide perovskites can easily exchange halide ions with the environment in different ways such as by immersing the perovskite in a reactive halide-based electrolyte solution or by exposing it to halogen gases [31,32]. The ion-exchange reaction always occurs rapidly even on perovskite nanostructures of different shape (films, rods, and nanoparticles) with the preservation of the structure and crystallinity of the material [33,34]. However, the replacement reaction may or not require an activation agent depending on the nature of the halogen source. The process can occur due to some peculiar qualities that characterize the halide perovskite derivatives such as fast ion migration ability [35], fast surface ion exchange and the possible coexistence of different ions (Cl^-, Br^- and I^-) in the same crystallographic site [36,37]. Unfortunately, the ease of the doping can also cause unwanted exchange effects.

To gain a deeper understanding of the antisolvent effect on the precipitation process, including the purity and the morphological properties of the final product, a fast crystallization screening has been performed by using the antisolvent diffusion method. A series of solvents were tested as precipitation agent to grow $MAPbBr_3$ crystals from DMF solutions. These trials have confirmed the effectiveness of ether and chlorinated systems to generate good quality millimetre-sized crystals in a relatively short time. However, in the samples containing dichloromethane an unexpected development has been observed consisting in a gradual but visible change over time of the crystals' colour from orange to yellow due to the substitution of Br by Cl. As described above for all the exchange experiments involving perovskites, the process takes places with the retention of the integrity of the single crystals and their morphologies and without loss of the samples' crystallinity (Fig. 3).

To confirm the bromide-chloride ion-exchange reaction and evaluate the degree of conversion, the samples were checked performing powder XRD measurements on ground crystals. The diffraction patterns show the typical peaks of the cubic Br phase characterised by a small shift toward a greater diffraction angle with the increase of the Cl concentration (Fig. 4).

A similar occurrence triggered by light has been recently observed in caesium lead halide nanocrystals $CsPbX_3$ (X = Cl, Br) dispersed in dihalomethane [38]. In this case the reaction occurs through a reductive dissociation of the solvent molecules with the produce of halide anions

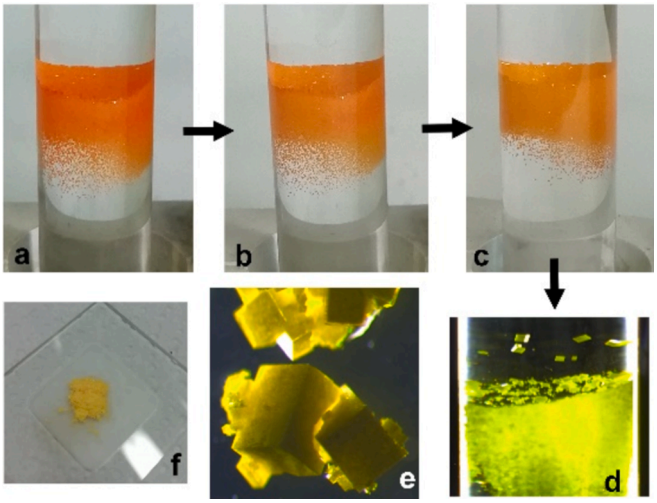

Fig. 3. From a) to d): progressive change in the colour of $MAPbBr_3$ crystals from dark orange to yellow disclosing a halogen exchange process between bromide and chloride ions. The process takes place in presence of dichloromethane solvent. e) Crystals of $MAPbBr_3$ obtained from a DMF-CH_2Cl_2 mixture by liquid/liquid diffusion method turned yellow during storage while retaining the crystal morphology (crystal size up to about 2 mm). f) Powder sample from ground crystals analysed by X-ray diffraction (XRD).

following the photoinduced interfacial electron transfer from excited perovskite [39].

To assess the reproducibility of phenomena and the conditions favourable to the Br-Cl substitution a series of experiments were performed in the presence of different chlorinated solvents such as chloroform and 1,2-dichloroethane that can act as source of chloride anions as observed in other cases [40]. Although the experimental results did not allow to understand the mechanism of the exchange process some useful information could be gleaned about the conditions favourable to the halogen anion replacement in the perovskite lattice. The main findings are that the halogen-exchange reaction works only in dichloromethane – DMF mixtures, it takes very long times to reach a visible grade of conversion and apparently it does not require light for activation although the process is clearly slower in dark environments.

Contrary to what one may expect, the transformation occurs faster for growing crystals than for powder samples, although the process does not occur uniformly throughout the entire crystallization trials as evidenced by the different shade of the yellowish-orange colour observed for the crystals and by the presence of multiple closely spaced Bragg diffraction peaks observed in some powder diffraction patterns corresponding to perovskite having different Cl/Br compositions (Fig. S4).

Because the effects of ion-exchange with the surrounding media may be not so evident it is important to identify the triggering factors to avoid unwanted interference with the growth environment. Further studies are needed to clarify the phenomena and elucidate the mechanism.

3.4. Impurity and crystalline stability

Beyond the halogen-exchange process, other issues negatively affecting the crystallization process have been observed. These include the formation of impurities and by-products as well as phenomena of product degradation. For these reasons the status of perovskite was monitored throughout the process.

In this way, a foreign phase, easily identified as lead bromide – DMF solvate [41] (Fig. S2), has been detected in initially pure powder samples after a time interval of some weeks. This is probably due to DMF and antisolvent absorbed on the surface of the powder that induce the degradation of the material leading to the formation and precipitation of $PbBr_2$(DMF) system [42]. However, a proper thermal treatment and a

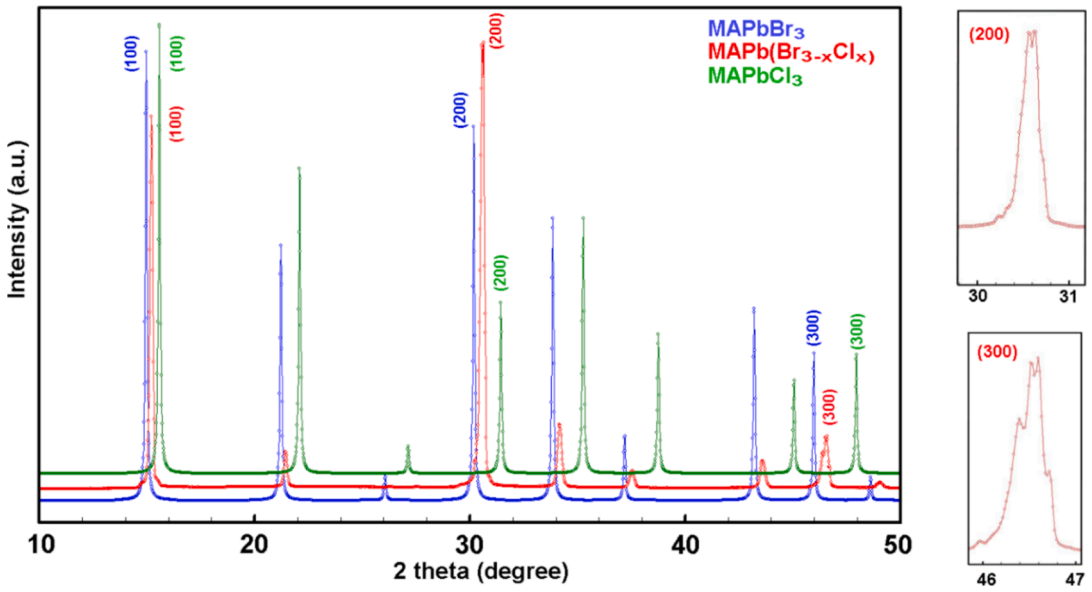

Fig. 4. Left: Intensity-normalized X-ray diffraction patterns of ground MAPb($Br_{3-x}Cl_x$) "yellow" crystals (red) compared to calculated single crystal data of $MAPbBr_3$ (blue) and $MAPbCl_3$ (green).The shift of the peaks to higher scattering angle 2θ is due to the halide exchange in the perovskite lattice. Right: The local magnification plot of the diffraction (200) and (300) peaks showing the splitting of reflections in multiple peaks indicating different grade of Cl-Br substitution present in the sample.

suitable drying can improve the stability of these materials over time.

Another small impurity has been detected in some XRD patterns of samples of ground crystals and attributed to the PbBr(OH) species (Fig. S3) [43]. Although $MAPbBr_3$, unlike the iodine species, do not show degradation after exposure to humidity, the use of non-anhydrous DMF solvent and the moisture uptake can promote the reaction with water leading to precipitation of sparingly soluble species, namely PbBr(OH) and $PbBr_2$ [44]. To determine the effect of water content in DMF and the moisture uptake into the crystallization solution a large volume of a dilute solution of perovskite was left standing in air to evaporate the solvent. After about one month a small amount of a white solid formed at the bottom of the flask which was collected by filtration and dried. The PXRD pattern confirmed that the solid corresponds to PbBr(OH). These results evidence the need to investigate and consider the effect on the final product of the presence of trace of water in the starting material and in the solvent and/or the direct exposure of the crystallization solution to the atmosphere. Indeed, experiments performed on various organic solvents indicate that the water content of a "dry" solvent can quickly increase over time under a nitrogen atmosphere in different relative humidity environments (DMF, 22 ± 2 °C, 50 % humidity, $[H_2O] = 30 \times 10^{-3}$ mol · L^{-1} after 120 min) [45].

Finally, it was noted that the XRD patterns of most of the crystalline powder samples show the presence of a series of unidentified peaks indicating a secondary phase. In most cases, the peaks are visible only at very high magnification of the intensity-2θ profiles or when the diagram is plotted in a semi-log scale as shown in Fig. 5. Only in a few cases some small peaks of the foreign phase emerge from the background and could be detected. In particular, the two peaks located at 2θ value of about 13.4° and 27.1°, are always recognisable but do not correspond to any known phase. However, the overall set of spurious peaks shows a periodicity typical of cubic crystals corresponding to a unit cell slightly smaller than that of perovskite (5.8 Å).

The trace presence of a crystalline guest indicated by the same diffraction peaks observed in the present work has been already reported in the literature [46]. The secondary phase has been associated with the formation of a new in-between phase $CH_3NH_3Br{\cdot}PbBr_2{\cdot}DMF$ or $PbBr_2{\cdot}DMF$ adduct complex, that self-assemble into a perovskite-type $PbBr_2$ within the $MAPbBr_3$ matrix [47,48].

No hypothesis can be completely confirmed or refuted, but some findings of the present work may be helpful in clarifying this issue. The most important observation is probably the presence of the spurious peaks also in the powder XRD spectra performed on single crystal samples. This could indicate that the problem is generated by the distortion of the structure at the interface probably determined by the evaporation of the MABr from the surface layers.

4. Conclusions

In the present work a crystal growth procedure has been proposed to efficiently produce good-quality perovskite single crystals in dimethylformamide by inverse temperature crystallization method. This technique is simple but demands a careful control of variety of parameters, including environmental and operational factors such as moisture or total reaction time, to ensure high products reproducibility between batches and over time. Phenomena of interfacial instability and possible material degradation connected to the process or environmental conditions have been highlighted and discussed as well as the efficient self-repair ability of this systems. Moreover, some aspects concerning the phase, and the structural purity of the samples were highlighted and assessed.

The temperature raising method is clearly a method not limited to laboratory-scale approaches, but precise control of crystallization factors is important in delineating the feasibility and scale-up of this technology at the industrial level. In this regard the reported results may be useful for the development of perovskite systems at the technological level and find a strategy to extend the durability and sustainability of devices based on hybrid perovskites.

CRediT authorship contribution statement

Silvia Rizzato: Writing – review & editing, Writing – original draft, Methodology, Investigation, Data curation, Conceptualization. **Marianna Testa:** Supervision, Funding acquisition. **Massimo Moret:** Writing – review & editing, Conceptualization.

Declaration of competing interest

The authors declare that they have no known competing financial

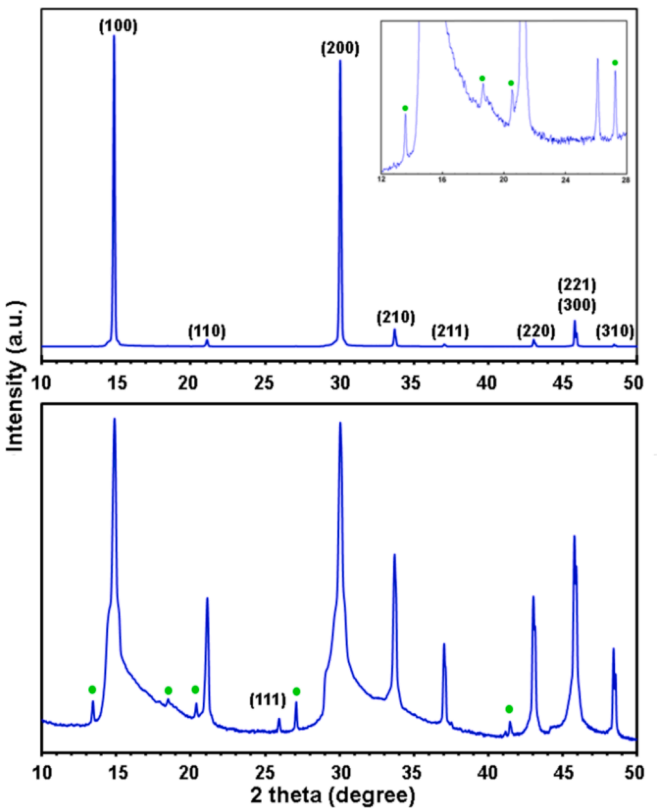

Fig. 5. (a) The PXRD pattern of a powder sample of $CH_3NH_3PbBr_3$ that shows quite sharp peaks at 14.96°, 21.22°, 30.08°, 33.74°, 37.04°, 43.06°, 45.98° and 48.44° corresponding to the (1 0 0), (1 1 0), (2 0 0), (2 1 0), (2 1 1), (2 2 0), (0 0 3) and (3 1 0) planes of the cubic crystal structure. The inset figure shows a magnification of the 10 – 30° 2θ range where small diffraction peaks emerge from the amorphous background (b) The same PXRD spectra plotted in a semi-log scale clearly indicating the presence of anonymous peaks at 13.45°, 18.54°, 20.46°, 27.18°, 41.48° of 2θ (green dots). In particular, the spurious peaks at 13.45° and 27.18° are visible to a greater or lesser extent in most samples (synthetised powders, ground crystals, crystal's slices) but cannot be assigned to any known phase.

interests or personal relationships that could have appeared to influence the work reported in this paper.

Acknowledgments

The authors thank M. Pegoraro and S. Vitali for their valuable technical assistance. The authors acknowledge financial support by the INFN – Commissione Scientifica Nazionale 5, Italy (Project: PEROV - R&D for photodetectors based on Organo-Metal Halide Perovskite material).

Appendix A. Supplementary material

Supplementary data to this article can be found online at https://doi.org/10.1016/j.jcrysgro.2025.128067.

Data availability

The authors do not have permission to share data.

References

[1] Y. Zhao, K. Zhu, Organic–inorganic hybrid lead halide perovskites for optoelectronic and electronic applications, Chem. Soc. Rev. 45 (2016) 655–689, https://doi.org/10.1039/C4CS00458B.
[2] Y. Dang, D. Ju, L. Wang, X. Tao, Recent progress in the synthesis of hybrid halide perovskite single crystals, CrstEngComm 18 (2016) 4476–4484, https://doi.org/10.1039/C6CE00655H.
[3] H. Zhang, X. Liu, J. Dong, H. Yu, C. Zhou, B. Zhang, Y. Xu, W. Jie, Centimeter-sized inorganic lead halide perovskite $CsPbBr_3$ crystals grown by an improved solution method, Cryst. Growth Des. 17 (12) (2017) 6426–6431, https://doi.org/10.1021/acs.cgd.7b01086.
[4] Y. Li, Z.-F. Shi, S. Li, L.-Z. Lei, H.-F. Ji, D. Wu, T.-T. Xu, Y.-T. Tian, X.-J. Li, High-performance perovskite photodetectors based on solution-processed all-inorganic $CsPbBr_3$ thin films, J. Mater. Chem. C 5 (2017) 8355–8360, https://doi.org/10.1039/C7TC02137B.
[5] W.A. Dunlap-Shohl, Y. Zhou, N.P. Padture, D.B. Mitzi, Synthetic Approaches for halide perovskite thin films, Chem. Rev. 119 (5) (2019) 3193–3295, https://doi.org/10.1021/ACS.CHEMREV.8B00318.
[6] Y. Lu, K. Qu, T. Zhang, Q. He, J. Pan, Metal halide perovskite nanowires: controllable synthesis, mechanism, and application in optoelectronic devices, Nanomaterials 13 (3) (2023) 419, https://doi.org/10.3390/NANO13030419.
[7] L. Protesescu, S. Yakunin, M.I. Bodnarchuk, F. Krieg, R. Caputo, C.H. Hendon, R. X. Yang, A. Walsh, M.V. Kovalenko, Nanocrystals of cesium lead halide perovskites ($CsPbX_3$, X = Cl, Br, and I): novel optoelectronic materials showing bright emission with wide color gamut, Nano Lett. 15 (6) (2015) 3692–3696, https://doi.org/10.1021/nl5048779.
[8] J. Shamsi, A.S. Urban, M. Imran, L. De Trizio, L. Manna, Metal halide perovskite nanocrystals: synthesis, post-synthesis modifications, and their optical properties, Chem. Rev. 119 (5) (2019) 3296–3348, https://doi.org/10.1021/ACS.CHEMREV.8B00644.
[9] M. Shi, R. Li, C. Li, Halide perovskites for light emission and artificial photosynthesis: opportunities, challenges, and perspectives, EcoMat 3 (1) (2021) e12074, https://doi.org/10.1002/eom2.12074.
[10] Y. Rong, Y. Hu, A. Mei, H. Tan, M.I. Saidaminov, S. Il Seok, M.D. McGehee, E. H. Sargent, H. Han, Challenges for commercializing perovskite solar cells, Science 361 (2018) eaat8235, https://doi.org/10.1126/science.aat8235.
[11] A.K. M. R., A. Nekahi, M.D. Bouguern, D. Ma, K. Zaghib, Advancements and challenges in perovskite-based photo-induced rechargeable batteries and supercapacitors: a comparative review, Batteries 10 (8) (2024) 284, doi: 10.3390/batteries10080284.
[12] M.A. Haque, J. Troughton, D. Baran, Processing-performance evolution of perovskite solar cells: from large grain polycrystalline films to single crystals, Adv. Energy Mater. 10 (13) (2020) 1902762, https://doi.org/10.1002/aenm.201902762.
[13] T.M. Brenner, D.A. Egger, L. Kronik, G. Hodes, D. Cahen, Hybrid organic—inorganic perovskites: low-cost semiconductors with intriguing charge-transport properties, Nat. Rev. Mater. 1 (2016) 15007, https://doi.org/10.1038/natrevmats.2015.7.
[14] M.I. Saidaminov, A.L. Abdelhady, B. Murali, E. Alarousu, V.M. Burlakov, W. Peng, I. Dursun, L. Wang, Y. He, G. Maculan, A. Goriely, T. Wu, O.F. Mohammed, O. M. Bakr, High-quality bulk hybrid perovskite single crystals within minutes by inverse temperature crystallization, Nat. Commun. 6 (2015) 7586, https://doi.org/10.1038/ncomms8586.
[15] Y. Liu, Z. Yang, D. Cui, X. Ren, J. Sun, X. Liu, J. Zhang, Q. Wei, H. Fan, F. Yu, X. Zhang, C. Zhao, S. (Frank) Liu, Two-inch-sized perovskite $CH_3NH_3PbX_3$ (X = Cl, Br, I) crystals: growth and characterization, Adv. Mater. 27 (35) (2015) 5176–5183, doi: 10.1002/adma.201502597.
[16] M. Testa, A. De Santis, G. Tinti, A. Paoloni, G. Papalino, G. Felici, Z. Chubinidze, F. Matteocci, M. Auf der Maur, S. Rizzato, L. Lo Presti, I. Viola, S. Morganti, C. Rovelli, Direct detection of minimum ionizing charged particles in a perovskite single crystal detector with single particle sensitivity, Nanoscale 16 (2024) 12918–12922, https://doi.org/10.1039/D4NR01556H.
[17] J. Rodriguez-Carvajal, FULLPROF: A program for Rietveld refinement and pattern-matching analysis, in: Abstracts of the Meeting Powder Diffraction, Toulouse, France, (1990)127–128.
[18] C.R. Groom, I.J. Bruno, M.P. Lightfoot, S.C. Ward, The Cambridge structural database, Acta Crystallogr. B Struct. Sci. Cryst. Eng. Mater. 72 (part 2) (2016) 171–179, https://doi.org/10.1107/S2052520616003954.
[19] A. Bonadio, J.A. Souza, Hybrid $MAPbI_3$ perovskite growth mechanism from irregular particles to cuboid and hopper-type morphologies, J. Braz. Chem. Soc. 33 (11) (2022) 1273–1280, https://doi.org/10.21577/0103-5053.20220057.
[20] B. Zhang, F. Guo, L. Yang, X. Jia, B. Liu, Z. Xie, D. Chen, H. Lu, R. Zhang, Y. Zheng, Shape-evolution control of hybrid perovskite $CH_3NH_3PbI_3$ crystals via solvothermal synthesis, J. Cryst. Growth 459 (2017) 167–172, https://doi.org/10.1016/J.JCRYSGRO.2016.12.014.
[21] Y. Chen, S. Yang, X. Chen, Y.C. Zheng, Y. Hou, Y.H. Li, H.D. Zeng, H.G. Yang, Direct insight into crystallization and stability of hybrid perovskite $CH_3NH_3PbI_3$via solvothermal synthesis, J. Mater. Chem. A 3 (2015) 15854–15857, https://doi.org/10.1039/C5TA03616J.
[22] E. Gu, X. Tang, S. Langner, P. Duchstein, Y. Zhao, I. Levchuk, V. Kalancha, T. Stubhan, J. Hauch, H.J. Egelhaaf, D. Zahn, A. Osvet, C.J. Brabec, Robot-based high-throughput screening of antisolvents for lead halide perovskites, Joule 4 (8) (2020) 1806–1822, https://doi.org/10.1016/j.joule.2020.06.013.
[23] K. Sangwal, Etching of Crystals. Theory, Experiment, and Application. North-Holland, Amsterdam 1987, pp. 43–86.
[24] R.C. Snyder, M.F. Doherty, Faceted crystal shape evolution during dissolution or growth, AIChE J. 53 (2007) 1337–1348, https://doi.org/10.1002/aic.11132.
[25] I. Sunagawa, (ed.) Morphology of Crystal, Part A and B, Terra Sci. Pub. Co., Tokyo and D. Reidel Publ. Co., Dordrecht, 1987.

[26] M.B. Al-Handawi, G. Dushaq, P. Commins, D.P. Karothu, M. Rasras, L. Catalano, P. Naumov, Autonomous reconstitution of fractured hybrid perovskite single crystals, Adv. Mater. 34 (19) (2022) 2109374, https://doi.org/10.1002/adma.202109374.
[27] S.K. Yadavalli, Z. Dai, H. Zhou, Y. Zhou, N.P. Padture, Facile healing of cracks in organic–inorganic halide perovskite thin films, Acta Mater. 187 (2020) 112–121, https://doi.org/10.1016/J.ACTAMAT.2020.01.040.
[28] S. Parida, S. Kumar, S. Cherf, S. Aharon, D. Cahen, B. Eren, Self-healing and -repair of nanomechanical damages in lead halide perovskites, Adv. Funct. Mater. 33 (45) (2023) 2304278, https://doi.org/10.1002/adfm.202304278.
[29] M. Budayova-Spano, F. Dauvergne, M. Audiffren, T. Bactivelane, S. Cusack, A methodology and an instrument for the temperature-controlled optimization of crystal growth, Acta Crystallogr. D D 63 (2007) 339–347, https://doi.org/10.1107/S0907444906054230.
[30] S. Pimputkar, S. Kawabata, J.S. Speck, S. Nakamura, Surface morphology study of basic ammonothermal GaN grown on non-polar GaN seed crystals of varying surface orientations from m-plane to a-plane, J. Cryst. Growth 368 (2013) 67–71, https://doi.org/10.1016/j.jcrysgro.2013.01.022.
[31] A. Efrati, S. Aharon, M. Wierzbowska, L. Etgar, First evidence of macroscale single crystal ion exchange found in lead halide perovskites, EcoMat 2 (1) (2020) e12016, https://doi.org/10.1002/eom2.12016.
[32] D. Solis-Ibarra, I.C. Smith, H.I. Karunadasa, Post-synthetic halide conversion and selective halogen capture in hybrid perovskites, Chem. Sci. 6 (2015) 4054–4059, https://doi.org/10.1039/C5SC01135C.
[33] D.M. Jang, K. Park, D.H. Kim, J. Park, F. Shojaei, H.S. Kang, J.-P. Ahn, J.W. Lee, J. K. Song, Reversible halide exchange reaction of organometal trihalide perovskite colloidal nanocrystals for full-range band gap tuning, Nano Lett. 15 (8) (2015) 5191–5199, https://doi.org/10.1021/acs.nanolett.5b01430.
[34] E. Belarbi, M. Vallés-Pelarda, B. Clasen Hames, R.S. Sanchez, E.M. Barea, H. Maghraoui-Meherzi, I. Mora-Seró, Transformation of PbI_2, $PbBr_2$ and $PbCl_2$ salts into $MAPbBr_3$ perovskite by halide exchange as an effective method for recombination reduction, Phys. Chem. Chem. Phys. 19 (2017) 10913–10921, https://doi.org/10.1039/C7CP01192J.
[35] Y. Yuan, J. Huang, Ion migration in organometal trihalide perovskite and its impact on photovoltaic efficiency and stability, Acc. Chem. Res. 49 (2) (2016) 286–293, https://doi.org/10.1021/acs.accounts.5b00420.
[36] J.H. Noh, S.H. Im, J.H. Heo, T.N. Mandal, S. Il Seok, Chemical management for colorful, efficient, and stable inorganic–organic hybrid nanostructured solar cells, Nano Lett. 13 (4) (2013) 1764–1769, doi: 10.1021/nl400349b.
[37] N.K. Kumawat, A. Dey, A. Kumar, S.P. Gopinathan, K.L. Narasimhan, D. Kabra, Band gap tuning of $CH_3NH_3Pb(Br_{1-x}Cl_x)_3$ hybrid perovskite for blue electroluminescence, ACS Appl. Mater. Interfaces 7 (24) (2015) 13119–13124, https://doi.org/10.1021/acsami.5b02159.
[38] D. Parobek, Y. Dong, T. Qiao, D. Rossi, D.H. Son, Photoinduced anion exchange in cesium lead halide perovskite nanocrystals, J. Am. Chem. Soc. 139 (12) (2017) 4358–4361, https://doi.org/10.1021/jacs.7b01480.
[39] L. Wang, G.D. Yuan, R.F. Duan, F. Huang, T.B. Wei, Z.Q. Liu, J.X. Wang, J.M. Li, Tunable bandgap in hybrid perovskite $CH_3NH_3Pb(Br_{3-y}X_y)$ single crystals and photodetector applications, AIP Adv 6 (4) (2016) 045115, https://doi.org/10.1063/1.4948312.
[40] Y. Zhang, F. Fadaei Tirani, P. Pattison, K. Schenk-Joß, Z. Xiao, M.K. Nazeeruddin, P. Gao, Zero-dimensional hybrid iodobismuthate derivatives: from structure study to photovoltaic application, Dalton Trans. 49 (2020) 5815–5822, https://doi.org/10.1039/D0DT00015A.
[41] K.L. Isakovskaya, I.A. Nikovskii, Y.V. Nelyubina, New low-dimensional perovskites based on lead bromide, Russ. J. Coord. Chem. 47 (2021) 365–375, https://doi.org/10.1134/S1070328421060026.
[42] F. Chen, C. Xu, Q. Xu, Y. Zhu, F. Qin, W. Zhang, Z. Zhu, W. Liu, Z. Shi, Self-assembled growth of ultrastable $CH_3NH_3PbBr_3$ perovskite milliwires for photodetectors, ACS Appl. Mater. Interfaces 10 (30) (2018) 25763–25769, https://doi.org/10.1021/acsami.8b05664.
[43] H.D. Lutz, K. Beckenkamp, T. Kellersohn, H. Möller, S. Peter, Neutron and X-ray structure determination of Laurionite-type Pb{O(H,D)}X, with X= Cl, Br, and I, hydrogen bonds to lead(II) ions as a hydrogen-bond acceptor, J. Solid State Chem. 124 (1) (1996) 155–161, https://doi.org/10.1006/jssc.1996.0219.
[44] K.K. Liu, Q. Liu, D.W. Yang, Y.C. Liang, L.Z. Sui, J.Y. Wei, G.W. Xue, W.B. Zhao, X. Y. Wu, L. Dong, C.X. Shan, Water-induced $MAPbBr_3$@PbBr(OH) with enhanced luminescence and stability, Light Sci. Appl. 9 (2020) 44, https://doi.org/10.1038/s41377-020-0283-2.
[45] Y. Hui, R.D. Webster, Absorption of water into organic solvents used for electrochemistry under conventional operating conditions, Anal. Chem. 83 (3) (2011) 976–981, https://doi.org/10.1021/ac102734a.
[46] W. Jiang, H. Di, H. Sun, C. Zhao, F. Liao, Y. Zhao, Role of DMSO concentration in the crystallization process of $MAPbBr_3$ perovskite single crystal films, J. Cryst. Growth 550 (2020) 125880, https://doi.org/10.1016/j.jcrysgro.2020.125880.
[47] Z. Ahmad, A. Mishra, Growth of $PbBr_2$ microrods with unique structure and surface morphology, J. Mater. Sci.: Mater. Electron. 31 (2020) 4672–4676, https://doi.org/10.1007/s10854-020-03019-0.
[48] F. Chen, C. Xu, Q. Xu, Y. Zhu, Z. Zhu, W. Liu, X. Dong, F. Qin, Z. Shi, Structure evolution of $CH_3NH_3PbBr_3$ single crystal grown in *N*,*N*-dimethylformamide solution, Cryst. Growth. Des. 18 (5) (2018) 3132–3137, https://doi.org/10.1021/acs.cgd.8b00256.